One-step preparation of coaxial CdS–ZnS and Cd1–xZn xS–ZnS nanowires

ARTICLE *in* ADVANCED FUNCTIONAL MATERIALS · JULY 2005

Impact Factor: 11.81 · DOI: 10.1002/adfm.200400563

3 AUTHORS, INCLUDING:

Shih-Yuan Lu
National Tsing Hua University
156 PUBLICATIONS **2,995** CITATIONS
SEE PROFILE

Yi-Feng Lin
Chung Yuan Christian University
49 PUBLICATIONS **889** CITATIONS
SEE PROFILE

ADVANCED FUNCTIONAL MATERIALS

FULL PAPER

One-Step Preparation of Coaxial CdS–ZnS and $Cd_{1-x}Zn_xS$–ZnS Nanowires**

By *Yung-Jung Hsu*, *Shih-Yuan Lu*,* and *Yi-Feng Lin*

Preparation of coaxial (core–shell) CdS–ZnS and $Cd_{1-x}Zn_xS$–ZnS nanowires has been achieved via a one-step metal–organic chemical vapor deposition (MOCVD) process with co-fed single-source precursors of CdS and ZnS. Single-source precursors of CdS and ZnS of sufficient reactivity difference were prepared and paired up to form coaxial nanostructures in a one-step process. The sequential growth of ZnS on CdS nanowires was also conducted to demonstrate the necessity and advantages of the precursor co-feeding practice for the formation of well-defined coaxial nanostructures. The coaxial nanostructure was characterized and confirmed by high-resolution transmission electron microscopy and corresponding energy dispersive X-ray spectrometry analyses. The photoluminescence efficiencies of the resulting coaxial CdS–ZnS and $Cd_{1-x}Zn_xS$–ZnS nanowires were significantly enhanced compared to those of the plain CdS and plain $Cd_{1-x}Zn_xS$ nanowires, respectively, owing to the effective passivation of the surface electronic states of the core materials by the ZnS shell.

1. Introduction

Semiconductor material as one-dimensional nanostructures have drawn much research attention in recent years owing to the novel properties, such as lasing action[1] and highly polarized photoluminescence,[2] that result from their particular dimensionality. It is generally accepted that one-dimensional nanostructures serve as a unique system for investigating the dependence of thermal, electrical, electronic, and optical properties on dimensionality and structure sizes. Their potential applications as building blocks, interconnects, and functional units in electronic and optoelectronic devices and sensors have also been demonstrated.[3] In recent years, the main effort in preparing one-dimensional nanomaterials has focused on the architecture of well-defined heterostructures, such as coaxial core–shell,[4] superlattice,[5] and composite[6] nanostructures. Materials with heterostructures often exhibit superior or new functional properties compared to their individual constituent materials. For coaxial nanowires, in general, multistep depositions involving sequential charges of desired source materials[4a,7] or surface modifications with ambient species[8] were necessary to acquire the correct architecture. Nevertheless, one-step processes for preparing coaxial nanowires have also been developed.[4b,4c,9–11] These processes involve vapor generation, transport, and deposition of co-fed target materials. Such practices, however, inevitably require high temperatures or high-vacuum laser-ablation operations in order to generate sufficient vapor for later deposition. We present herein a chemical vapor deposition (CVD)-based approach for coaxial nanowire preparation that can be conducted at much lower temperatures. Coaxial (core–shell) CdS–ZnS and $Cd_{1-x}Zn_xS$–ZnS nanowires were successfully prepared in a one-step metal–organic CVD (MOCVD) process by co-feeding molecular, single-source precursors of CdS and ZnS of suitable reactivity mismatch.

Among the many one-dimensional nanostructured semiconductor materials, nanowires of binary Group II–VI and III–V compounds, such as ZnO, CdS, ZnS, and GaN have been extensively studied.[12] Although much research has been done on the electrical and optical properties of one-dimensional binary semiconductor compounds, much less information is available for ternary systems of one-dimensional nanostructures. It has been shown that some ternary semiconductor compounds possess even better properties than the corresponding binary compounds,[13] and, by adjusting the stoichiometry of the constituent components, their properties can be effectively tuned.[14] For example, ternary $Cd_{1-x}Zn_xS$ nanocrystals are known to possess properties falling between those of CdS and ZnS, and a color-tunable emission of nanocrystals of the alloy $Cd_{1-x}Zn_xS$ can be achieved by adjusting the composition ratio of cadmium to zinc.[15] In addition, by incorporating ZnS, $Cd_{1-x}Zn_xS$ acquires a larger energy bandgap than CdS, making the material much more attractive for applications in solar cells and photoconductive devices.[16] Herein, we report the successful synthesis of ternary sulfide, $Cd_{1-x}Zn_xS$, nanowires and coaxial $Cd_{1-x}Zn_xS$–ZnS nanowires. These nanowires were formed by adjusting the deposition temperature in a one-step MOCVD process appropriately, to invoke the in-situ alloying of CdS and ZnS immediately after the formation of the coaxial CdS–ZnS nanowires.

Previously, the practice of co-feeding precursors has been utilized to achieve co-deposition of TiO_2–SiO_2 composite particle films and in-situ surface passivation of CdS nanoparticles with ZnS shells.[17] Recently, we successfully incorporated the precursor co-feeding practice with the vapor–liquid–solid

[*] Prof. S.-Y. Lu, Y.-J. Hsu, Y.-F. Lin
Department of Chemical Engineering, National Tsing-Hua University
Hsinchu, Taiwan 30043 (Taiwan)
E-mail: sylu@mx.nthu.edu.tw

[**] Financial support from the National Science Council of the Republic of China under grant NSC-93-2214-E-007-010 is gratefully acknowledged.

  DOI: 10.1002/adfm.200400563

ADVANCED FUNCTIONAL MATERIALS

(VLS)[18] growth mechanism for one-dimensional nanostructures, and achieved a one-step preparation of coaxial CdS–ZnS nanowires.[19] Dialkyldithiocarbamate-based single-source precursors of CdS ($Cd(S_2CN(C_3H_7)_2)_2$, denoted as Cd33) and ZnS ($[Zn(S_2CNBu_2)_2]_2$, denoted as Zn44), were synthesized and co-fed into the reactor. The co-fed precursors of CdS and ZnS were designed to possess a sufficient reactivity difference to enable sequential reaction for the in-situ formation of the core–shell structure.[17] We ran the deposition at 280 °C separately for Cd33 and Zn44 and found only CdS nanowires were produced from the VLS growth mechanism and no ZnS deposits were formed at all. However, when Cd33 and Zn44 were co-fed into the system, a deposition run, again at 280 °C, gave nanowires composed of both CdS and ZnS. This observation implies that Zn44 reacted to form ZnS in the presence of CdS nanowires. In other words, based on the reactivity difference existing between Cd33 and Zn44, Cd33 was thermally decomposed first to form the core CdS nanowires via the VLS mechanism in the presence of a gold catalyst, and these first-formed nanowires then served as the catalyst to promote the thermal decomposition of Zn44. As a result, the later-formed ZnS grew on the surface of the first-formed CdS nanowires, and thus a one-step fabrication of coaxial nanowires was successfully achieved.[19]

We also examined the growth when the two precursors were introduced into the system sequentially, to make comparisons with the precursor co-feeding practice. The effect of the co-feeding practice on the morphology of the resulting nanowires, as well as the corresponding optical properties, was investigated and is discussed. By controlling the deposition temperature, ZnS in the shell region alloyed with the CdS core, leading to formation of the ternary alloy $Cd_{1-x}Zn_xS$ nanowires coated with a thin layer of remaining ZnS. Further increasing the deposition temperature resulted in the formation of single-phase $Cd_{1-x}Zn_xS$ nanowires because of the complete consumption of ZnS in the in-situ alloying process. With this development, we were able to observe a photoluminescence band resulting from the alloy of CdS and ZnS. This finding offers an alternative route for adjusting the photoluminescence performance of one-dimensional semiconductor nanowires—by alloying with suitable materials.

2. Results and Discussion

At a deposition temperature of 280 °C, single feeding of Cd33 gave CdS nanowires 20–30 nm in diameter and several micrometers long. Figure 1a shows a transmission electron microscopy (TEM) image of a single CdS nanowire with a diameter of about 30 nm. The dark region at the wire tip (Fig. 1a, inset) is the gold catalyst, confirming the VLS mechanism. The dot pattern of the corresponding selected-area electron diffraction (SAED) pattern (Fig. 1b) suggests that the plain CdS nanowires grew as a single crystal. The SAED pattern can be indexed to the reflection of hexagonal CdS crystals along the [001] direction. Figure 1c shows the high-resolution TEM (HRTEM) image of the region marked in Figure 1a. The clear

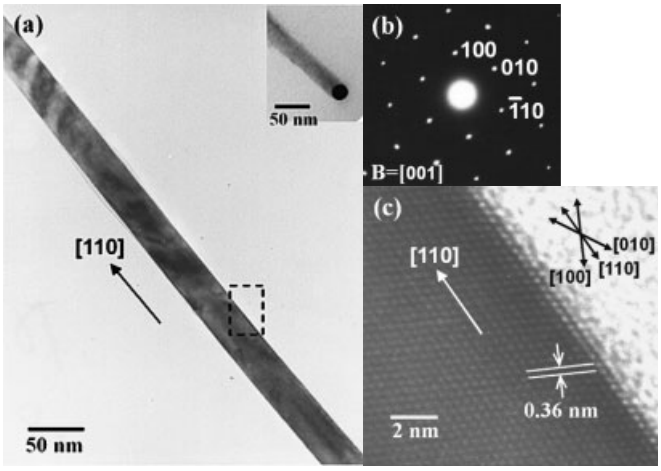

Figure 1. Plain CdS nanowires prepared at 280 °C. a) Low-magnification TEM image; b,c) the corresponding SAED pattern and HRTEM image, respectively, of the region marked in (a).

lattice fringes in this image confirm the single-crystal structure of the CdS nanowires. The lattice spacing of 0.36 nm corresponds to the *d*-spacing of the (100) planes of hexagonal CdS ($d(100) = 0.358$ nm for bulk hexagonal CdS). The axis of the CdS nanowire is parallel to the [110] direction, indicating that the CdS nanowires grew along the [110] direction.

Co-feeding of Cd33 and Zn44 at a deposition temperature of 280 °C, however, led to the formation of coaxial CdS–ZnS nanowires. Typical bright-field and dark-field TEM images of a single CdS–ZnS nanowire are shown in Figures 2a,b, respectively. The apparent contrast between the inner core and the outer shell suggests the existence of a coaxial structure. The contrast can be more clearly seen in Figure 2c, an HRTEM image of a section of the coaxial nanowire. The shell layer is about 10 nm thick; the diameter of the core is around 30 nm. From the TEM–energy dispersive X-ray (EDX) analyses (Fig. 3), only zinc and sulfur were found in the projected shell region; in the projected core region, cadmium was richer than zinc, accompanied by an approximately stoichiometric amount of sulfur. This further confirmed the coaxial structure of the CdS–ZnS nanowires. Note that in the projected shell region, only the ZnS shell was sampled, whereas in the projected core region, both the CdS core and ZnS shell were probed—but the thicker core contributed more than the thinner shell. In Figure 2d, the SAED pattern of the coaxial CdS–ZnS nanowire taken at the marked region of Figure 2c was composed of two sets of diffraction patterns. These were indexed with dots as hexagonal CdS and rings as cubic ZnS crystals, respectively. The lattice-resolved HRTEM image of the region marked in Figure 2c is shown in Figure 2e. The ZnS shell has an interlayer spacing of 0.31 nm, which agrees well with the lattice spacing of the (111) planes of cubic ZnS ($d(111) = 0.312$ nm for bulk cubic ZnS); the CdS core gave a 0.32 nm interlayer spacing, which is in agreement with the lattice spacing of the (101) planes of hexagonal CdS ($d(101) = 0.316$ nm for bulk hexagonal CdS). The closeness of the two lattice spacings enabled the

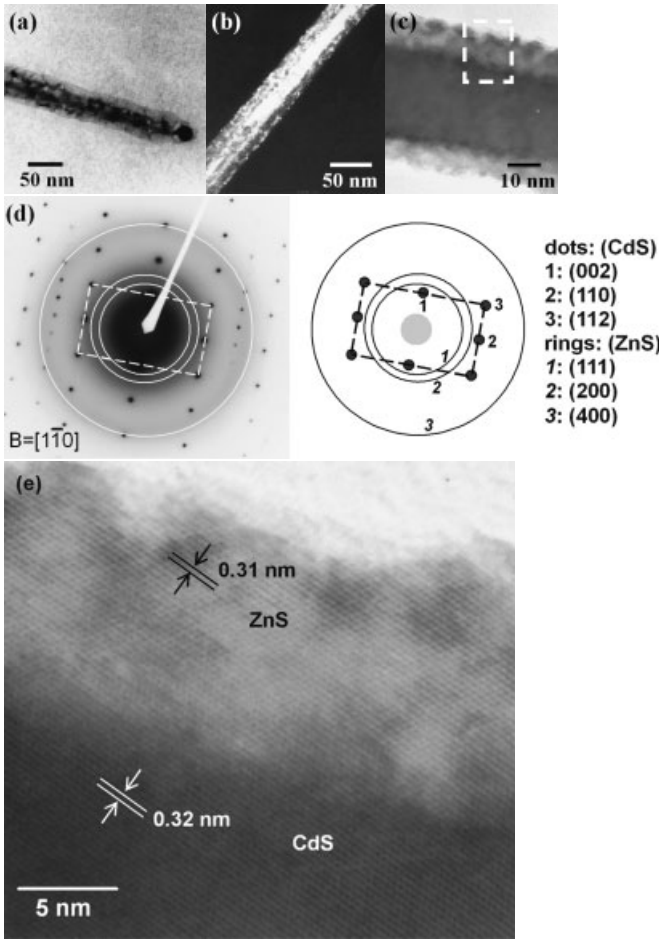

Figure 2. Coaxial CdS–ZnS nanowires prepared at 280 °C. a,b) Typical bright-field and dark-field TEM images, respectively; c) HRTEM image showing the coaxial nanostructure; d,e) the corresponding SAED pattern and enlarged HRTEM image, respectively, of the region marked in (c).

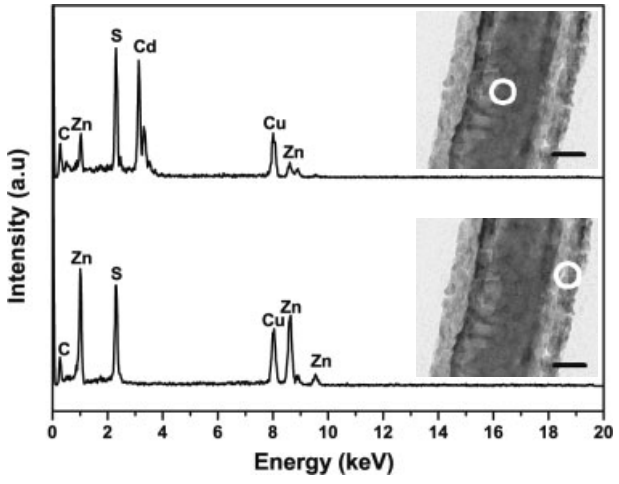

Figure 3. TEM–EDX analyses of the projected shell and core regions of a single coaxial CdS–ZnS nanowire; two inset scale bars = 10 nm.

ZnS shell to grow on the CdS core via a minor atomic-level surface reconstruction.

To examine further the validity of our proposal that the CdS nanowires served as a catalyst, promoting the subsequent formation of ZnS, we performed a sequential growth. The two precursors were introduced into the system sequentially. CdS nanowires were formed at a deposition temperature of 280 °C by the VLS mechanism via the single feeding of Cd33. Precursor Zn44 was then introduced into the system at the same deposition temperature. The morphology of the resulting nanowires is shown in the TEM image of Figure 4a. The CdS nanowires formed from in first stage were stained with a large quantity of ZnS nanoparticles on their surfaces. The presence

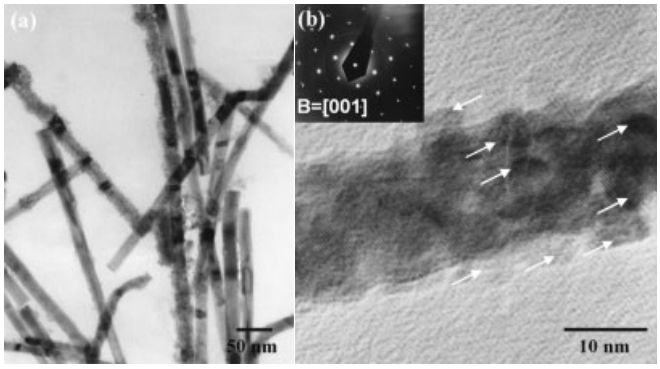

Figure 4. Sequentially grown CdS–ZnS nanowires prepared at 280 °C. a) Low-magnification TEM image; b) HRTEM image showing that the CdS nanowire was stained with many ZnS nanoparticles (indicated by arrows). The inset is the corresponding SAED pattern.

of elemental zinc was confirmed by TEM–EDX analyses. The existence of ZnS nanoparticles on the surfaces of CdS nanowires can be more clearly seen in Figure 4b, indicated by the arrows. The SAED image (Fig. 4b, inset) shows the single-crystallinity of the CdS core in the dot pattern, and the existence of the cubic ZnS in the ring pattern. In addition, the ZnS nanoparticles grew only on the surfaces of the CdS nanowires. In other regions, such as the substrate surfaces, no ZnS deposits were found. This observation further confirms our proposal that the CdS nanowires served not only as the template,[20] but also the catalyst for the subsequent ZnS formation.

The effect of the precursor co-feeding practice on the morphology of the resulting nanowires was also examined. Sequential precursor feeding led to an incomplete and particle-film-like coating on the surfaces of the CdS nanowires; precursor co-feeding resulted in an epitaxially grown shell with smooth surfaces and a uniform thickness. Precursor co-feeding was indispensable for the formation of well-defined coaxial nanostructures in this work.

The UV-vis absorption spectra of the coaxial CdS–ZnS nanowires, sequentially grown CdS–ZnS nanowires, and plain CdS nanowires are shown together in Figure 5a, for comparison. For the plain CdS nanowires, an absorption edge at around 500 nm is evident, conforming to the energy bandgap of 2.5 eV of CdS.[21] The absorption spectrum of the sequentially grown CdS–ZnS nanowires is dominated by the CdS core, and there is

ADVANCED FUNCTIONAL MATERIALS

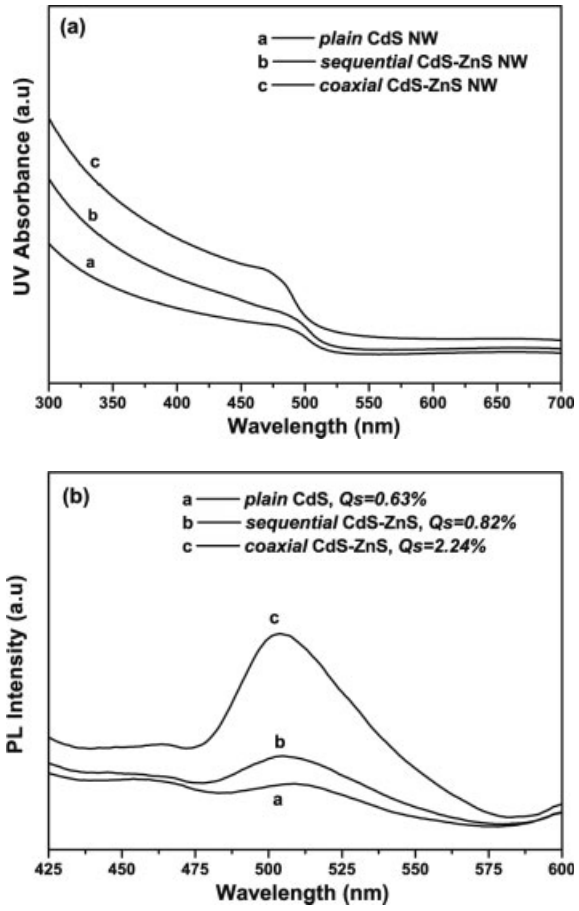

Figure 5. a) UV-vis absorption and b) room-temperature PL emission spectra of the coaxial CdS–ZnS nanowires, compared with those of sequentially grown CdS–ZnS and plain CdS nanowires; the excitation wavelength was 320 nm.

a slight blue-shift in the absorption edge, due to the influence of the ZnS nanoparticles coated on the surfaces of the CdS core.[17b] The blue-shift in the absorption edge was more pronounced for the coaxial CdS–ZnS nanowires, indicating a complete and thicker coverage of ZnS on CdS. The corresponding photoluminescence (PL) spectra are compared in Figure 5b. The three samples showed a typical near-edge emission of CdS with the peaks centered around 500–510 nm. The sequentially grown and coaxial CdS–ZnS nanowires basically exhibited the PL behavior of the CdS core, with the ZnS shell playing a modification role. The passivation of the surface electronic states[17b,22] of the CdS core by the ZnS nanoparticle coating led to a slight enhancement in PL intensity and quantum yields (Q) for the sequentially grown CdS–ZnS nanowires over the corresponding plain CdS nanowires. This enhancement was much more dramatic for the coaxial CdS–ZnS nanowires owing to the complete coverage, and thus more effective passivation, of the ZnS shell on the CdS core.

The influence of deposition temperature on the morphology, crystal structure, and corresponding optical properties of the resulting composite nanowires was also investigated. On increasing the deposition temperature from 280 to 400 °C, or even 500 °C, while keeping all other reaction conditions fixed, the composite CdS–ZnS nanowires grew much thicker in diameter to around 100 nm (as shown below, Figs. 8b,9a). The composite nanowires grew up to over 1 μm long, as shown in Figures 6a,b for deposition temperatures of 400 and 500 °C, respectively.

In Figure 7, we present the X-ray diffraction (XRD) patterns of the composite CdS–ZnS nanowires, obtained from deposition temperatures of 400 and 500 °C. Also included in Figure 7 are the XRD patterns of the ZnS thin films produced at a deposition temperature of 500 °C, reference hexagonal CdS (Joint Committee on Powder Diffraction Standards (JCPDS) file no. 06-0314), reference ternary $Cd_{0.72}Zn_{0.28}S$ (JCPDS file no. 40-0836), reference ternary $Cd_{0.22}Zn_{0.78}S$ (JCPDS file no. 35-1469), and reference cubic ZnS (JCPDS file no. 05-0566), for comparison. The composite CdS–ZnS nanowires showed

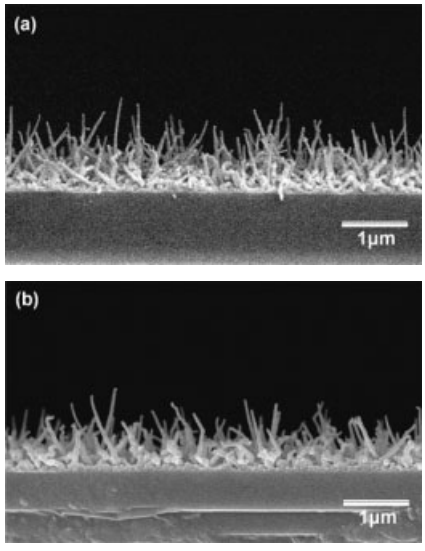

Figure 6. Cross-sectional scanning electron microscopy (SEM) images of the composite CdS–ZnS nanowires prepared at a) 400 °C and b) 500 °C.

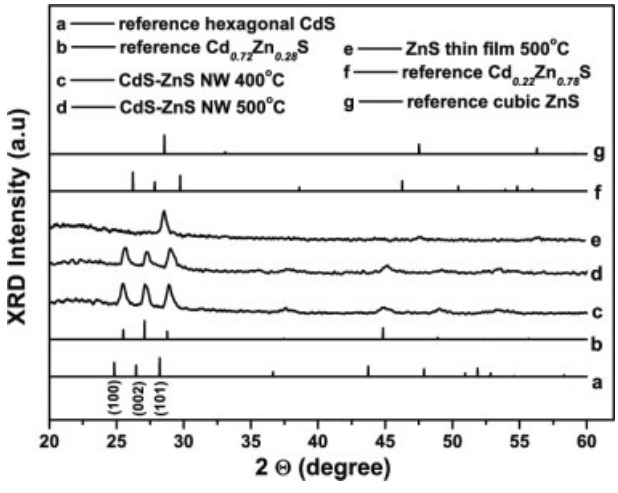

Figure 7. XRD patterns of composite CdS–ZnS nanowires prepared at 400 °C and 500 °C compared with those of ZnS thin films, reference hexagonal CdS, reference $Cd_{0.72}Zn_{0.28}S$, reference $Cd_{0.22}Zn_{0.78}S$, and reference cubic ZnS.

predominantly the diffraction behavior of hexagonal CdS, with an apparent right-shift of the three main peaks due to the alloying with ZnS. The crystal structures of the composite nanowires were neither pure CdS nor pure ZnS. The positions of the three main diffraction peaks were located between those of ternary $Cd_{0.72}Zn_{0.28}S$ and $Cd_{0.22}Zn_{0.78}S$ crystals, indicating the formation of $Cd_{1-x}Zn_xS$, an alloy of CdS and ZnS, in the composite nanowires. Lattice spacings of the crystallographic planes were calculated on the basis of the XRD patterns, according to Bragg's law. For composite CdS–ZnS nanowires prepared at 400 °C, the three main diffraction peaks at 2θ of 25.54, 27.21, and 28.92° correspond to the (100), (002), and (101) planes with *d*-spacings of 0.348, 0.327, and 0.308 nm, respectively. For composite CdS–ZnS nanowires prepared at 500 °C, the peaks at 2θ of 25.69, 27.38, and 29.15° gave interplanar spacings of 0.346, 0.325, and 0.306 nm for the (100), (002), and (101) planes, respectively. The detailed crystallographic structures were later investigated by TEM and HRTEM.

For the samples prepared at 400 °C, an evident contrast between the core and the shell was also observed, as shown in the TEM images of Figures 8a,b. TEM–EDX analyses showed that zinc was much richer than cadmium in the projected shell region, whereas in the projected core region, both cadmium and zinc were identified with an atomic composition ratio of about 58:42 for Cd/Zn. Note that the shell region was too narrow (less than 5 nm thick) to ensure a shell-only sampling during the TEM–EDX analysis for the projected shell region. Thus, the minor cadmium signal may be a contamination from the core region. This issue can be further clarified in the SAED and HRTEM analyses. In Figure 8c, the corresponding SAED image taken at the edge of a single nanowire was composed of two sets of diffraction patterns, with dots for the hexagonal ternary $Cd_{1-x}Zn_xS$ and rings for the cubic ZnS crystals, respectively. The lattice-resolved HRTEM image taken at the edge of a single coaxial $Cd_{1-x}Zn_xS$–ZnS nanowire is shown in Figure 8d. The interface between the core and shell is highlighted with a dashed line. The average shell thickness is about 4 nm. The ZnS shell showed an interlayer spacing of 0.31 nm, which agrees well with the lattice spacing of the (111) planes of cubic ZnS; the core gave an 0.35 nm interlayer spacing—in good agreement with the lattice spacing of the (100) planes of the hexagonal $Cd_{1-x}Zn_xS$, as determined from the XRD analysis ($d(100) = 0.348$ nm). The axis of the nanowire is parallel to the [100] direction, indicating that the $Cd_{1-x}Zn_xS$ nanowires grew along the [100] direction. The above analyses suggest that the composite CdS–ZnS nanowires prepared at 400 °C also possess coaxial nanostructures, with ternary $Cd_{1-x}Zn_xS$ as the core coated with a thin layer of ZnS. In addition, structural deformations, such as vacancies and stacking faults (SFs) are present in the crystal structures, as indicated by the dashed circles in Figure 8d. The two insets in Figure 8d are enlarged HRTEM images that more clearly reveal the vacancies and SFs.

For the composite CdS–ZnS nanowires prepared at a deposition temperature of 500 °C, no significant diffraction contrast, which would suggest the existence of a core–shell structure, was found—as evident in the TEM image, Figure 9a. TEM–EDX analyses showed a uniform elemental composition along the radial direction of the nanowires with an atomic composi-

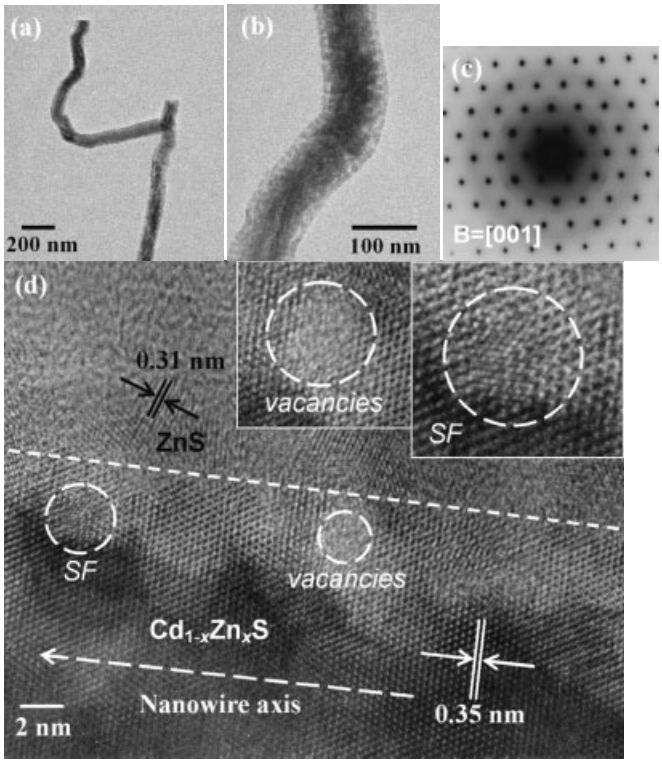

Figure 8. Coaxial $Cd_{1-x}Zn_xS$–ZnS nanowires prepared at 400 °C. a) Low-magnification TEM image; b) HRTEM image showing the coaxial nanostructure; c) the corresponding SAED image recorded along the [001] zone axis; d) HRTEM image taken at the edge of a single composite nanowire. The interface between the two semiconductor layers is highlighted with a dashed line. The insets are two enlarged HRTEM images showing more clearly the vacancies and stacking faults.

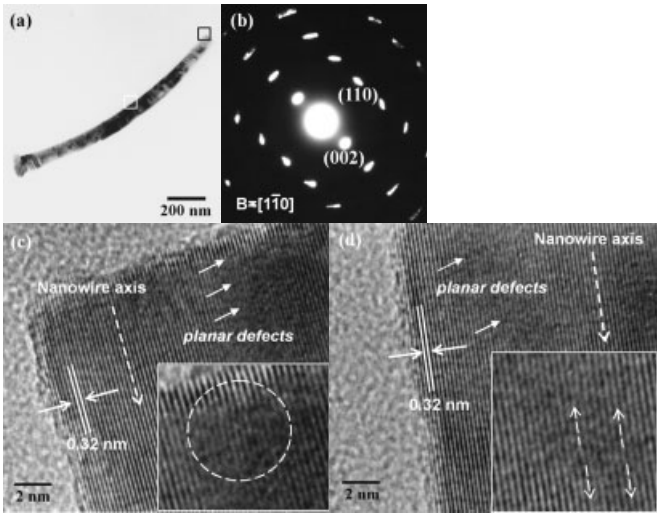

Figure 9. Single-phase ternary $Cd_{1-x}Zn_xS$ nanowires prepared at 500 °C. a) TEM image of a single $Cd_{1-x}Zn_xS$ nanowire; b) the corresponding SAED image with the zone axis of [1$\bar{1}$0]; c,d) HRTEM images of the tip and stem regions, respectively, marked in (a), with enlarged inset HRTEM images showing the planar defects.

ADVANCED FUNCTIONAL MATERIALS

tion ratio of about 55:45 for Cd/Zn. The variation in diffraction contrast along the nanowire length was due to the existence of structural deformations.[23] The stretched spots in the SAED images (Fig. 9b) were probably caused by the planar deformations existing in the crystals. The lattice-resolved images taken from the tip and stem regions, as marked in Figure 9a, are shown in Figures 9c,d, respectively. The spacing between two neighboring fringes is about 0.32 nm, in good agreement with the interplanar spacing of the (002) planes of ternary $Cd_{1-x}Zn_xS$, and consistent with the value determined from the corresponding XRD analysis ($d(002) = 0.325$ nm). Planar defects were found, and these are indicated by the arrows in Figures 9c,d. The insets show enlarged HRTEM images, to more clearly illustrate the defects. The identical lattice fringe patterns of both the tip and stem regions imply that the ternary $Cd_{1-x}Zn_xS$ nanowires were formed with a uniform chemical composition and good quality of crystallinity along the growth axis during the alloying process, with no other materials, such as ZnS remaining on the nanowire surfaces.

The UV-vis absorption spectra of the coaxial $Cd_{1-x}Zn_xS$–ZnS nanowires and single-phase $Cd_{1-x}Zn_xS$ nanowires are shown in Figure 10a. For the coaxial $Cd_{1-x}Zn_xS$–ZnS nanowires prepared at 400 °C, an absorption edge at around 440 nm, corresponding to a direct energy bandgap of 2.82 eV, was evident. The same energy bandgap of 2.82 eV was observed by Kumar et al., who grew $Cd_{0.6}Zn_{0.4}S$ thin films by a vacuum evaporation process.[24] The single-phase $Cd_{1-x}Zn_xS$ nanowires show a slight blue-shift, to around 430 nm ($E_g = 2.88$ eV), in their absorption edge, due to the complete alloying of ZnS with CdS. As expected, an increase in energy bandgap was observed in both composite nanowire samples containing $Cd_{1-x}Zn_xS$, as compared to plain CdS nanowires ($E_g = 2.5$ eV). The bulk bandgap energy, $E_g(x)$, of an alloy A_xB_{1-x} can be expressed by Equation 1[25]

$$E_g(x) = E_B + (E_A - E_B - b)x + bx^2 \text{ [eV]} \quad (1)$$

where b is the bowing parameter and x is the atomic fraction of compound A. The value of b was found to be about 0.61 eV for the $Cd_{1-x}Zn_xS$ alloy.[14a,26] The bulk bandgap energy for ternary $Cd_{1-x}Zn_xS$ alloys thus increased nonlinearly with increasing atomic ratio of Zn/(Zn + Cd) (x) according to Equation 2

$$E_g(x) = 2.5 + 0.59x + 0.61x^2 \text{ [eV]} \quad (2)$$

By substituting the observed bandgap energies of 2.82 and 2.88 eV into Equation 2, the theoretical atomic ratios of Zn/(Zn + Cd) for the alloy $Cd_{1-x}Zn_xS$ nanowires prepared at 400 and 500 °C were estimated to be about 0.39 and 0.44, respectively. The atomic ratio of Zn/(Zn + Cd) can also be estimated from the corresponding TEM–EDX analyses. A value of 0.45 was thus obtained for the single-phase $Cd_{1-x}Zn_xS$ nanowires, in good agreement with that estimated from Equation 2. For the coaxial $Cd_{1-x}Zn_xS$–ZnS nanowires prepared at 400 °C, a thin layer of pure ZnS coated on the surfaces of the $Cd_xZn_{1-x}S$ nanowires accounted for the excess zinc observed (0.42 from the TEM–EDX versus 0.39 from Equation 2).

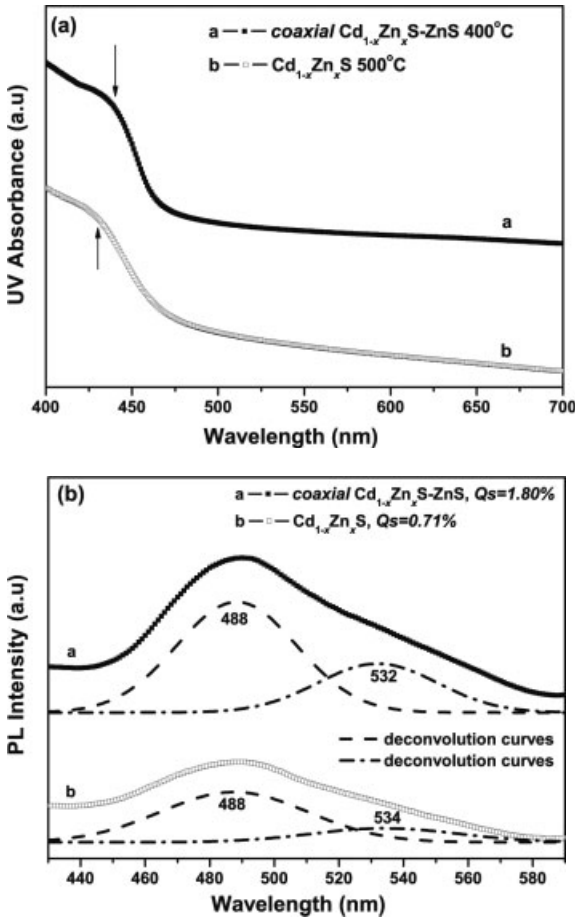

Figure 10. a) UV-vis absorption and b) room-temperature PL emission spectra of the coaxial $Cd_{1-x}Zn_xS$–ZnS nanowires compared with that of the plain $Cd_{1-x}Zn_xS$ nanowires. The absorption edges are indicated by the arrows. PL spectra (solid lines) were deconvoluted into two Gaussian distributions (dashed lines). The excitation wavelength was 320 nm.

The corresponding PL spectra are compared in Figure 10b. A rather broad emission band, ranging from 440–580 nm, was observed in both single-phase $Cd_{1-x}Zn_xS$ and coaxial $Cd_{1-x}Zn_xS$–ZnS nanowires. Peak deconvolution with Gaussian distributions showed that the both broad bands were composed of two sub-bands centered around 488 nm and 532 nm. For most semiconductor crystals, two types of emission band are usually observed: one due to excitonic emission, and the other due to trap-state emission. Excitonic emission is sharp and is located near the absorption edge; trap-state emission is broad and is located at longer wavelengths.[27] Ray et al. observed an emission peak located at around 490 nm in their $Cd_{0.6}Zn_{0.4}S$ thin films obtained from a vacuum evaporation process.[16a] Their results suggest that the shorter wavelength emission band (488 nm) of this work originates from the excitonic emission of the ternary $Cd_{1-x}Zn_xS$ alloy via the radiative band-to-band recombination process, whereas the longer wavelength band (532 nm) comes from the trap-state emission. For the near-edge emission band at around 488 nm, both the PL intensity and quantum yields were enhanced for the coaxial $Cd_{1-x}Zn_xS$–ZnS nanowires, as compared to those for the single-phase

$Cd_{1-x}Zn_xS$ nanowires. This enhancement can be attributed to the effective surface passivation of $Cd_{1-x}Zn_xS$ by ZnS,[28] similar to that observed in coaxial CdS–ZnS nanowires. The trap-state emission at around 532 nm probably came from the four types of point defects present in the nanowires.[29] Sulfur vacancies and zinc (cadmium) interstitials produced donor states, whereas vacancies of zinc (cadmium) and interstitials of sulfur led to acceptor states. In addition, other crystallographic defects, such as stacking faults and planar defects formed during the in-situ alloying process, as shown in Figure 8d and Figures 9c,d, may also induce defect-level emission in the PL spectra.[30]

A possible growth mechanism for the formation of the coaxial $Cd_{1-x}Zn_xS$–ZnS and single-phase $Cd_{1-x}Zn_xS$ nanowires is proposed as follows. At a deposition temperature of 400 °C, CdS nanowires (formed from the VLS mechanism) served as both the catalyst and template to induce the lateral growth of ZnS. Meanwhile, the CdS core and later-formed ZnS started to form alloys at the interface of CdS and ZnS owing to the higher deposition temperature of 400 °C (compared to 280 °C for the formation of the coaxial CdS–ZnS nanowires). The induced growth of ZnS turned out to be faster than the alloying of CdS with ZnS at 400 °C, thus leading to the formation of coaxial $Cd_{1-x}Zn_xS$–ZnS nanowires. On further increasing the deposition temperature, the alloying rate of CdS with ZnS bypassed the induced growth rate of ZnS, and thus single-phase $Cd_{1-x}Zn_xS$ resulted. Note that the surfaces of the $Cd_{1-x}Zn_xS$ nanowires still served as the catalyst and template for the further lateral growth and subsequent alloying of CdS with ZnS.

It might be argued that the composite CdS–ZnS nanowires obtained under the high deposition temperatures may be in the form of a uniform mixture of plain CdS and ZnS nanowires. To clarify this issue, MOCVD using Zn44 as the precursor in the presence of the gold catalyst was also conducted. Figure 11a shows the surface morphology of the resulting ZnS deposits on the gold-coated quartz substrates at a deposition temperature of 500 °C. Thin films were obtained instead of one-dimensional nanowires. The XRD pattern of the ZnS thin film (Fig. 7, curve e) exhibited peak positions corresponding to those of the cubic structures. Figure 11b shows a typical TEM image of a piece of the thin film. Some dots of darker contrast were observed to exist in the matrix domain, which can be more clearly seen in Figure 11c, an enlarged TEM image of the region marked in Figure 11b. From the TEM–EDX analyses, the dark-contrast dots were confirmed to be gold whereas the matrix domain was ZnS. The SAED pattern (Fig. 11c, inset) shows that ZnS grew as polycrystals of cubic zinc-blende structure.

It might also be argued that at higher deposition temperatures the alloy nanowires formed directly from the molecularly mixed precursors, without first forming the CdS core and then later coating and alloying ZnS. It has been demonstrated that, for the VLS growth mechanism, the characteristic size of the gold catalyst is strongly correlated with the diameter of the resulting one-dimensional structure.[31] In this work, even at the higher deposition temperature of 500 °C, some gold particles coalesced and grew only up to about 50 nm in diameter, as seen in Figure 11c. Gold particles of this size cannot explain the resulting diameter of about 100 nm for the alloy nanowires, however a mechanism in which the CdS core is formed first and then ZnS coating and alloying occur does.

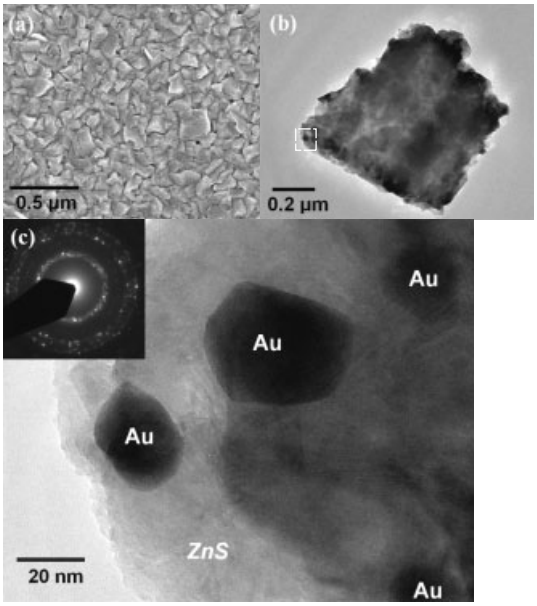

Figure 11. Au–ZnS composite thin films prepared at 500 °C. a) Top-view SEM image showing the morphology of the deposited films. b) Low-magnification TEM image of a piece of the thin film. c) High-magnification TEM image of the region marked in (b), showing gold particles embedded in the ZnS matrix; the inset is the SAED pattern, which reveals the polycrystallinity of the cubic ZnS.

3. Conclusions

We have successfully prepared coaxial CdS–ZnS and $Cd_{1-x}Zn_xS$–ZnS nanowires and achieved in-situ coating and in-situ alloying with a one-step MOCVD process by co-feeding two single-source precursors of sufficient reactivity difference on gold-sputtered substrates. The co-feeding of precursors was shown to be indispensable for forming well-defined coaxial nanostructures. The coaxial nanostructure was confirmed by HRTEM and EDX analyses at the projected core and shell regions. A PL quantum-yield enhancement, caused by the effective passivation of core materials by the ZnS shell, was observed in these one-dimensional coaxial nanostructures. By raising the deposition temperature to 400 °C, the ZnS shell alloyed with the CdS core, leading to the formation of ternary-alloy $Cd_{1-x}Zn_xS$ nanowires coated with a thin layer of ZnS; at the even higher deposition temperature of 500 °C, single-phase $Cd_{1-x}Zn_xS$ nanowires were obtained. With this development, we were able to observe a photoluminescence band resulting from the alloy of CdS and ZnS. This finding offers an alternative route to adjusting one-dimensional semiconductors' photoluminescence band structure, by alloying suitable materials. This novel synthetic technique is also expected to be applicable to the preparation of nanowires of other ternary semiconductor, or even ceramic, compounds.

4. Experimental

MOCVD Preparation of Coaxial CdS–ZnS, Coaxial $Cd_{1-x}Zn_xS$–ZnS, and Single-Phase $Cd_{1-x}Zn_xS$ Nanowires: MOCVD was conducted in a simple hot-wall reactor [17b]. Fused silica plates sputtered with gold were used as the substrates for growth of the nanowires. Dialkyldithiocarbamate-based [32] single-source precursors of CdS ($Cd(S_2CN(C_3H_7)_2)_2$, Cd33) and ZnS ($[Zn(S_2CNBu_2)_2]_2$, Zn44), were synthesized and co-fed into the reactor. The detailed synthetic methods and relevant characterization of the precursors used in this work can be found in our previous work [17b]. The two precursors were heated at different temperatures (Cd33 at 160 °C and Zn44 at 120 °C) to generate suitable amounts of precursor vapor. The vapors of both precursors were introduced into the furnace by N_2 carrier gas. The furnace temperatures were set at 280, 400, and 500 °C, for different experiment runs. Depositions were run at a carrier gas flow rate of 200 sccm, system pressure of 30 torr (1 torr = 133.32 Pa), and reaction time of 6 h. In addition, the sequential growth of ZnS on first-formed CdS nanowires was carried out at a deposition temperature of 280 °C with a 3 h deposition time. Plain CdS nanowires and plain ZnS thin films were prepared at 280 °C and 500 °C, respectively, for comparison purposes.

Characterization: The morphology and dimensions of the nanowires were examined using field-emission scanning electron microscopy (FESEM, Hitachi S-4700). The crystallographic structures of the nanowires were investigated with XRD (MAC Sience MXP18), TEM (TEM, JEOL JEM-2010), and HRTEM (JEOL JEM-400EX). The elemental analyses of individual nanowires were conducted with an EDX spectrometer, a TEM accessory (JEM-2010). UV-vis absorption spectra were obtained using a Hitachi U-3300 spectrophotometer. For PL spectroscopy, a Hitachi F-4500 equipped with a xenon lamp (150 W) and a 700 V photomultiplier tube as detector was used. The excitation wavelength was 320 nm. Both absorption and photoluminescence spectra were obtained at room temperature under an ambient atmosphere.

Received: December 3, 2004
Final version: March 5, 2005

[1] a) M. H. Huang, S. Mao, H. Feick, H. Yan, Y. Wu, H. Kind, E. Weber, R. Russo, P. Yang, *Science* **2001**, *292*, 1897. b) J. X. Ding, J. A. Zapien, W. W. Chen, Y. Lifshitz, S. T. Lee, *Appl. Phys. Lett.* **2004**, *85*, 2361.

[2] J. Wang, M. S. Gudiksen, X. Duan, Y. Cui, C. M. Lieber, *Science* **2001**, *293*, 1455.

[3] a) Y. Xia, P. Yang, Y. Sun, Y. Wu, B. Mayers, B. Gates, Y. Yin, F. Kim, H. Yan, *Adv. Mater.* **2003**, *15*, 353. b) Z. R. Dai, Z. W. Pan, Z. L. Wang, *Adv. Funct. Mater.* **2003**, *13*, 9.

[4] a) L. J. Lauhon, M. S. Gudiksen, D. Wang, C. M. Lieber, *Nature* **2002**, *420*, 57. b) Q. Li, C. Wang, *J. Am. Chem. Soc.* **2003**, *125*, 9892. c) J. Zhang, L. Zhang, F. Jiang, Y. Yang, J. Li, *J. Phys. Chem. B* **2005**, *109*, 151.

[5] a) M. S. Gudiksen, L. J. Lauhon, J. Wang, D. C. Smith, C. M. Lieber, *Nature* **2002**, *415*, 617. b) Y. Wu, R. Fan, P. Yang, *Nano Lett.* **2002**, *2*, 83. c) M. T. Björk, B. J. Ohlsson, T. Sass, A. I. Persson, C. Thelander, M. H. Magnusson, K. Deppert, L. R. Wallenberg, L. Samuelson, *Nano Lett.* **2002**, *2*, 87.

[6] a) K.-K. Lew, L. Pan, E. C. Dickey, J. M. Redwing, *Adv. Mater.* **2003**, *15*, 2073. b) J. Jie, G. Wang, X. Han, J. Fang, Q. Yu, Y. Liao, B. Xu, Q. Wang, J. G. Hou, *J. Phys. Chem. B* **2004**, *108*, 8249. c) J. Zhan, Y. Bando, J. Hu, T. Sekiguchi, D. Golberg, *Adv. Mater.* **2005**, *17*, 225.

[7] a) Y. Xie, P. Yan, J. Lu, Y. Qian, S. Zhang, *Chem. Commun.* **1999**, 1969. b) J. Cao, J.-Z. Sun, H.-Y. Li, J. Hong, M. Wang, *J. Mater. Chem.* **2004**, *14*, 1203. c) X. Liang, S. Tan, Z. Tang, N. A. Kotov, *Langmuir* **2004**, *20*, 1016. d) S. J. An, W. I. Park, G.-C. Yi, Y.-J. Kim, H.-B. Kang, M. Kim, *Appl. Phys. Lett.* **2004**, *84*, 3612. e) S. Han, C. Li, Z. Liu, B. Lei, D. Zhang, W. Jin, X. Liu, T. Tang, C. Zhou, *Nano Lett.* **2004**, *4*, 1241. f) J. Hwang, B. Min, J. S. Lee, K. Keem, K. Cho, M.-Y. Sung, M.-S. Lee, S. Kim, *Adv. Mater.* **2004**, *16*, 422.

[8] a) H.-M. Lin, Y.-L. Chen, J. Yang, Y.-C. Liu, K.-M. Yin, J.-J. Kai, F.-R. Chen, L.-C. Chen, Y.-F. Chen, C.-C. Chen, *Nano Lett.* **2003**, *3*, 537. b) J.-R. Kim, B.-K. Kim, J.-O. Lee, J. Kim, H. J. Seo, C. J. Lee, J.-J. Kim, *Nanotechnology* **2004**, *15*, 1397.

[9] a) J. L. Gole, J. D. Stout, W. L. Rauch, Z. L. Wang, *Appl. Phys. Lett.* **2000**, *76*, 2346. b) X. Y. Kong, Y. Ding, Z. L. Wang, *J. Phys. Chem. B* **2004**, *108*, 570.

[10] a) R. Ma, Y. Bando, *Chem. Mater.* **2002**, *14*, 4403. b) Y. Li, Y. Bando, D. Golberg, *Adv. Mater.* **2003**, *15*, 581. c) J. Hu, Y. Bando, Z. Liu, *Adv. Mater.* **2003**, *15*, 1000. d) Y. B. Li, Y. Bando, D. Golberg, *Chem. Phys. Lett.* **2003**, *375*, 102. e) Y.-C. Zhu, Y. Bando, D.-F. Xue, D. Golberg, *J. Am. Chem. Soc.* **2003**, *125*, 16 196. f) Y. Li, Y. Bando, D. Golberg, *Adv. Mater.* **2004**, *16*, 93.

[11] a) X.-M. Meng, J.-Q. Hu, Y. Jiang, C.-S. Lee, S.-T. Lee, *Appl. Phys. Lett.* **2003**, *83*, 2241. b) J. Q. Hu, Q. Li, X. M. Meng, C. S. Lee, S. T. Lee, *Chem. Mater.* **2003**, *15*, 305.

[12] a) M. H. Huang, Y. Wu, H. Feick, N. Tran, E. Weber, P. Yang, *Adv. Mater.* **2001**, *13*, 113. b) X. Duan, C. M. Lieber, *Adv. Mater.* **2000**, *12*, 298. c) C. J. Barrelet, Y. Wu, D. C. Bell, C. M. Lieber, *J. Am. Chem. Soc.* **2003**, *125*, 11 498. d) T. Kuykendall, P. Pauzauskie, S. Lee, Y. Zhang, J. Goldberger, P. Yang, *Nano Lett.* **2003**, *3*, 1063. e) Q. Xiong, G. Chen, J. D. Acord, X. Liu, J. J. Zengel, H. R. Gutierrez, J. M. Redwing, L. C. Lew Yan Voon, B. Lassen, P. C. Eklund, *Nano Lett.* **2004**, *4*, 1663. f) L. Dong, T. Gushtyuk, J. Jiao, *J. Phys. Chem. B* **2004**, *108*, 1617.

[13] a) A. Wang, J. Dai, J. Cheng, M. P. Chudzik, T. J. Marks, R. P. H. Chang, C. R. Kannewurf, *Appl. Phys. Lett.* **1998**, *73*, 327. b) D. L. Young, D. L. Williamson, T. J. Coutts, *J. Appl. Phys.* **2002**, *91*, 1464.

[14] a) B. A. Korgel, H. G. Monbouquette, *Langmuir* **2000**, *16*, 3588. b) X. Zhong, M. Han, Z. Dong, T. J. White, W. Knoll, *J. Am. Chem. Soc.* **2003**, *125*, 8589.

[15] a) D. V. Petrov, B. S. Santos, G. A. L. Pereira, C. D. M. Donegá, *J. Phys. Chem. B* **2002**, *106*, 5325. b) X. Zhong, Y. Feng, W. Knoll, M. Han, *J. Am. Chem. Soc.* **2003**, *125*, 13 559.

[16] a) S. C. Ray, M. K. Karanjai, D. DasGupta, *Thin Solid Films* **1998**, *322*, 117. b) M. E. Rincón, M. W. Martínez, M. Miranda-Hernández, *Sol. Energy Mater. Sol. Cells* **2003**, *77*, 25.

[17] a) S.-Y. Lu, S.-W. Chen, *J. Am. Ceram. Soc.* **2000**, *83*, 709. b) Y.-J. Hsu, S.-Y. Lu, *Langmuir* **2004**, *20*, 194.

[18] a) R. S. Wagner, W. C. Ellis, *Appl. Phys. Lett.* **1964**, *4*, 89. b) Y. Wu, P. Yang, *J. Am. Chem. Soc.* **2001**, *123*, 3165.

[19] Y.-J. Hsu, S.-Y. Lu, *Chem. Commun.* **2004**, 2102.

[20] a) R. He, M. Law, R. Fan, F. Kim, P. Yang, *Nano Lett.* **2002**, *2*, 1109. b) J. Hu, Y. Bando, Z. Liu, T. Sekiguchi, D. Golberg, J. Zhan, *J. Am. Chem. Soc.* **2003**, *125*, 11 306.

[21] a) S.-Y. Lu, M.-L. Wu, H.-L. Chen, *J. Appl. Phys.* **2003**, *93*, 5789. b) Y.-J. Hsu, S.-Y. Lu, *Langmuir* **2004**, *20*, 23.

[22] a) L. Manna, E. C. Scher, L.-S. Li, A. P. Alivisatos, *J. Am. Chem. Soc.* **2002**, *124*, 7136. b) T. Mokari, U. Banin, *Chem. Mater.* **2003**, *15*, 3955.

[23] Y. Ding, Z. L. Wang, *J. Phys. Chem. B* **2004**, *108*, 12 280.

[24] P. Kumar, A. Misra, D. Kumar, N. Dhama, T. P. Sharma, P. N. Dixit, *Opt. Mater.* **2004**, *27*, 261.

[25] R. Hill, *J. Phys. C* **1974**, *7*, 521.

[26] a) L. G. Suslina, E. I. Danasyuk, S. G. Konnikov, D. L. Federov, *Sov. Phys. Semicond.* **1976**, *10*, 1093. b) L. I. Berger, *Semiconductor Materials*, CRC Press, Boca Raton, FL **1997**.

[27] a) M. O'Neil, J. Marohn, G. McLendon, *J. Phys. Chem.* **1990**, *94*, 4356. b) J. Butty, N. Peyghambarian, Y. H. Kao, J. D. Mackenzie, *Appl. Phys. Lett.* **1996**, *69*, 3224.

[28] M. Nirmal, L. Brus, *Acc. Chem. Res.* **1999**, *32*, 407.

[29] a) D. Denzler, M. Olschewski, K. Sattler, *J. Appl. Phys.* **1998**, *84*, 2841. b) N. Pinna, K. Weiss, J. Urban, M.-P. Pileni, *Adv. Mater.* **2001**, *13*, 261.

[30] K.-W. Chang, J.-J. Wu, *Adv. Mater.* **2004**, *16*, 545.

[31] a) M. S. Gudiksen, C. M. Lieber, *J. Am. Chem. Soc.* **2000**, *122*, 8801. b) Y.-J. Hsu, S.-Y. Lu, *Appl. Phys. A*, **2005**, *81*, 573.

[32] a) P. O'Brien, J. R. Walsh, I. M. Watson, L. Hart, S. R. P. Silva, *J. Cryst. Growth* **1996**, *167*, 133. b) M. Motevalli, P. O'Brien, J. R. Walsh, I. M. Watson, *Polyhedron* **1996**, *15*, 2801.

